Flow, Turbulence and Combustion manuscript No.
(will be inserted by the editor)

The Effect of Wall Normal Actuation on a Turbulent Boundary Layer

S.C. Schlanderer · N. Hutchins · R.D. Sandberg

Received: date / Accepted: date

Abstract In this work, a series of direct numerical simulations are conducted to study the effect of wall normal spanwise homogeneous wall actuation on a turbulent boundary layer. The moving boundary is represented by a boundary data immersion technique. A parametric study was performed, varying the actuator length, the wall normal actuation amplitude and the actuation frequency. It was found that localized actuation, relying only on wall motion instead of requiring a plenum in the case of synthetic jets, generated a net momentum flux jet affecting the flow not only in the immediate vicinity of the actuator but also for a significant distance downstream. The cases with an actuator velocity of $u^+_{act} = 20.1$ showed a particularly pronounced effect on the boundary layer and resulted in a recirculation region.

Keywords wall normal actuation · flow control · turbulent boundary layer

1 Introduction

In the field of flow control for skin friction reduction, research into active wall deformations have tended to focus on spanwise wall oscillations and streamwise travelling waves. Spanwise waves have been shown to reduce skin friction drag by up to 25% for a turbulent boundary layer flow in a numerical study by Lardeau & Leschziner [8]. However, there is mounting evidence that this type of control becomes less effective for increasing Reynolds numbers [4]. Furthermore, spanwise travelling waves or wall oscillations are comparatively complicated to implement in an experimental setup and even more so at application type Reynolds number. Itoh et al. [5] and Tamano & Itoh [17] combined spanwise travelling waves with wall deformations of a flexible sheet and found a

S.C. Schlanderer · N. Hutchins · R.D. Sandberg
Fluids Group, University of Melbourne
E-mail: stefan.schlanderer@unimelb.edu.au

drag reduction of up to 8% in their experiments. Wall deformations of compliant coatings or surfaces have also been studied previously as a mean of passive flow control [9,19]. Active wall motion as an approach to flow control has been studied to delay transition by Jacobson & Reynolds [6] with cantilever vanes driven by piezo ceramics. For control of turbulent flows, wall normal deformation has received less attention despite the fact that it is considered very robust in rough environments [2] and is likely to be relatively easy to implement in practice. Kang & Choi [7] and Endo et al. [2] numerically considered a channel wall that could locally deform according to the control scheme they used and found $12 - 17\%$ drag reduction. In a recent experimental study Bai et al. [1] found a drag reduction of more than 30% compared to the unactuated case. The maximum drag reduction was observed for a spanwise uniform actuation, i.e. a spanwise wave length of infinity, even though they mentioned that their effective wave-length is likely to be smaller due to the experimental setup.
The present study considers spanwise uniform actuation in the wall normal direction of a turbulent boundary layer employing direct numerical simulations (DNS). The objective is to investigate the response of the turbulent flow to an actuation that is likely to be realizable with reasonable effort, at least in low to moderate Reynolds number laboratory measurements.

2 Computational Setup and Validation

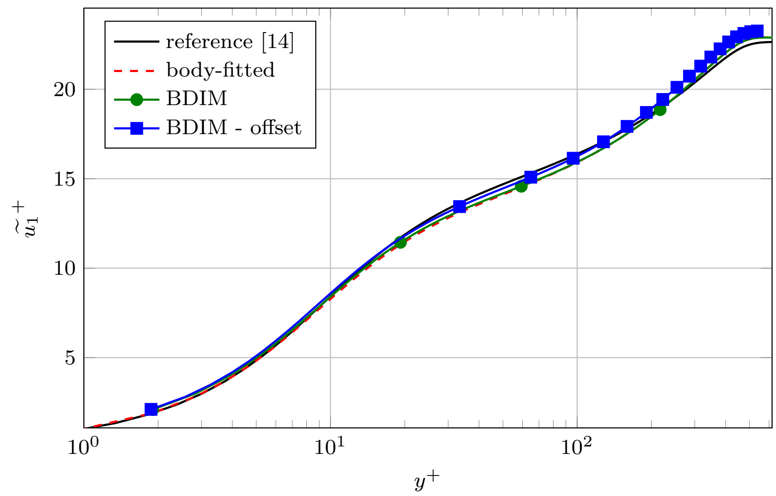

Fig. 1: Turbulent boundary layer velocity profile scaled with viscous units comparing the BDIM to the body-fitted boundary conditions and the reference data from [14]. In the simulation ‘BDIM - offset’ the wall location was not prescribed between two grid lines.

In the current work a fully compressible high-order Navier-Stokes DNS code is employed. Details about the code and numerical schemes can be found in reference [11]. The domain for the turbulent boundary layer incorporated the streamwise range of $1020 < Re_\theta < 1528$, where Re_θ is the Reynolds number based on momentum thickness. The Mach number was set to M=0.5 and the Prandtl number was Pr=0.72. The wall temperature was assumed to be isothermal at $T_{wall} = 1.05$ in non-dimensional units. The wall normal grid spacing was constant along the streamwise direction with a maximum wall grid spacing of $\Delta y^+ = 0.97$ based on local viscous units and stretched over 101 grid points towards the freestream boundary. In the streamwise direction the grid spacing was uniform with a maximum value of $\Delta x^+ = 18.0$ based on local viscous units. The wall normal and streamwise directions were discretized with a fourth-order accurate finite difference scheme. The spanwise domain height was $l_y \approx 29.5\delta^*_{in}$ and the width was $l_z \approx 8\delta^*_{in}$ where δ^*_{in} is the displacement thickness at the inflow. Based on the outflow displacement thickness δ^*_{out} the domain height was $l_y \approx 20.4\delta^*_{out}$ and the width was $l_z \approx 5.5\delta^*_{out}$. A spectral method with 32 Fourier modes was used to discretize the spanwise domain width which yields a spanwise grid spacing of $\Delta z^+ = 8.13$. At the inflow synthetic turbulent fluctuations, originating from the digital filter approach by Touber & Sandham [18], were superimposed to a mean turbulent velocity profile. The freestream and outflow boundary conditions were prescribed using characteristic boundary conditions. At the outflow a zonal characteristic boundary condition approach was employed [12].

The wall normal actuation was prescribed with a moving body employing the Boundary Data Immersion Method (BDIM) for compressible flows that was previously validated for aeroacoustic research [13] and successfully applied to fluid-structure interaction problems [16]. The concept of this method is to couple the fluid and the solid body domain through a smoothing region of half-width ϵ which is commonly and in this work set to $\epsilon = 2\Delta y^+$. The method's order of accuracy is increased by taking the wall normal gradient into account. For more details on the method the reader is referred to Schlanderer et al. [13].

Figure 1 compares the streamwise velocity profile scaled in viscous units from simulations obtained in the current study and incompressible reference data from reference [15]. It can be observed that the body fitted simulation shows slight deviations from the reference in the wake region. This can be attributed to the short and narrow domain and inflow length of the current case and the relatively low Reynolds number of $Re_\theta = 1410$. However, for the purpose of a comparison of the effect of different wall boundary conditions, i.e. body-fitted and immersed boundary, the agreement is reasonable. In addition, figure 1 compares the incompressible reference [14] and body-fitted boundary simulations to the BDIM approach with and without an offset of half a grid point from the original wall location. When the offset is zero the wall location coincides with the underlying grid. The offset of half a grid point places the wall between two grid lines such that the surface does not coincide with the

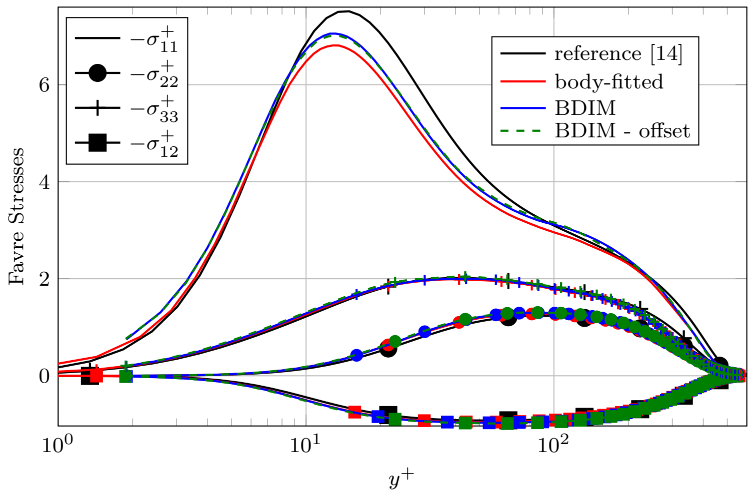

Fig. 2: Reynolds stress profiles in a turbulent boundary layer scaled with viscous units comparing the BDIM with and with out offset to the body-fitted boundary conditions and the reference data from reference [14].

underlying grid and the y^+ coordinate was corrected accordingly. For both BDIM cases the viscous units were derived using $\frac{\partial \widetilde{u_1}}{\partial x_2}$ evaluated at $y = \epsilon$, i.e. at the second grid point from the prescribe wall location, as the velocity gradient at the wall can inherently not be matched exactly by a continuous method. The comparison in figure 1 shows that the profiles of the case with and without offset hardly show any difference. Despite the fact that the offset to the original surface location is small, deviations could be identified when the wall normal coordinate was not corrected according to the offset. This demonstrates that the mean velocity profile can be represented very accurately even when the surface does not coincide with the underlying grid with an accuracy that is of the order of half a grid point. In addition, both BDIM cases show very good agreement with the reference case employing body-fitted boundary conditions with the same grid and inflow method.

The Favre averaged velocity fluctuation profiles for the same cases are presented in figure 2. The comparison of the body-fitted data and the reference [14] again shows some minor differences in particular for the streamwise component σ_{11}. This is due to the reasons noted earlier and for the sake of assessing the BDIM approach the agreement is seen as sufficiently good. When the wall is represented by the BDIM the shape of the profile as well as the amplitude is captured well for all components except the streamwise velocity fluctuations σ_{11}, where the amplitude is slightly overestimated. It was found that this deviation is due to a slightly overestimated value of $\frac{\partial \widetilde{u_1}}{\partial x_2}$ and vanishes when the profiles are scaled with viscous units derived from the body-fitted

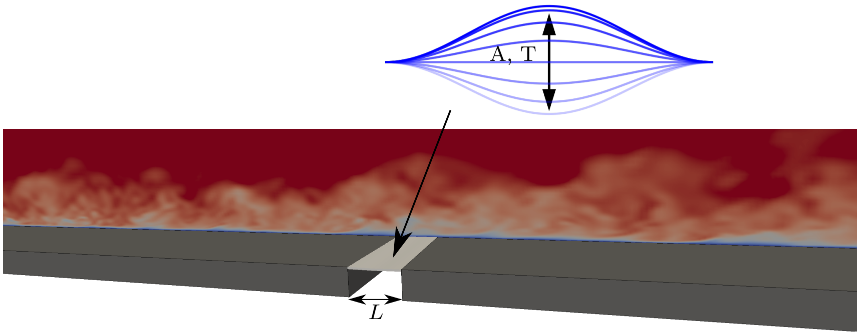

Fig. 3: Visualization of the computational setup where the flat plate is marked in dark grey and the actuator in light grey. The background is showing instantaneous contours of the streamwise velocity component. The parameters that were modified are the length of the actuator L as well as the actuation amplitude A and period T.

simulations. The cases with and without offset show perfect agreement in shape and amplitude of the velocity fluctuations, thus confirming the accuracy of the modelled wall location.
Overall, this shows that the BDIM is an appropriate method to represent a wall adjacent to a turbulent flow with high accuracy, independent of the underlying grid, and the exact location of the plate surface can be represented very accurately leading to a "sharp like" modelling of the surface.

Figure 3 visualizes the setup of the actuated boundary layer with the actuation parameters. In all cases that are discussed in this paper the actuator end was located at $Re_\theta = 1369$ of the undisturbed boundary layer with a baseline length of $L^+_{act} \approx 188$ which is comparable to the actuator length used by Bai et al. [1], although that study focused on a smaller Re_θ. It should be noted that the actuators employed by Bai et al. [1] were cantilever supported whereas our actuator has a trigonometric shape. They can be considered similar in how the fluid is actuated, i.e. accelerated towards or away from the wall. However, the wake of both actuator types will be different. In the current study the actuation was homogeneous in the spanwise direction. The BDIM was employed to impose the wall boundary condition upstream and downstream of the actuator to avoid spurious effects from the change of body-fitted to immersed boundary conditions. To that end 20 grid points were mirrored below the actual surface of the wall and initialized with zero velocity, uniform density and the wall temperature. For the simulations with the wall normal actuation the grid resolution was refined in the streamwise direction to $\Delta x^+ = 4.4$ at the actuator. Furthermore the wall normal grid spacing was constant for $-15 < y^+ < 15$ to accurately resolve the motion of the actuator.

3 Influence of Actuation Parameters and Actuator Length

The main objective of the current work is to study the effect of an actuation on the turbulent boundary layer. Skin friction drag reduction is used purely as a measure to quantify the changes in the boundary layer downstream of the actuation. In the following section the influence of different actuation parameters such as actuator length as well as actuation amplitude and period are evaluated. The most efficient actuation parameters found by Bai et al. [1] were employed as a starting point, despite differences in the exact shape of the actuator and the expected flow in the wake.

Figure 4 shows the change of skin friction compared to the unactuated boundary layer downstream of the actuator for different actuation parameters. The streamwise coordinate x^+ refers to the same physical location in all cases as x is scaled with the viscous units from the unactuated case. All of these parameters are variations around the parameters that were found to have the most significant effect by Bai et al. [1], namely an actuation amplitude of $A^+ \approx 2$ and an actuation period of $T^+ \approx 2.5$ for an actuator with a length of $L^+ \approx 140$. Figure 4a presents the spatial evolution of skin friction downstream of the actuator for different actuation periods. It is apparent that the actuator influence increases with shorter actuation periods when comparing the decrease of skin friction just downstream of the actuator. In addition the recovery towards the unactuated case seems to be slower for higher actuation frequencies. However, for the fastest actuation with an actuation period of $T^+ = 0.625$, which is faster than the viscous time scale, a very high reduction can be found which is then followed by a higher skin friction. The general trend that a higher actuation frequency leads to a lower skin friction and thus greater change in the turbulent flow is partly consistent with the results measured by Bai et al. [1]. However, in their data the effectiveness in reducing skin friction seem to level off at actuation periods lower than $T^+ = 2.5$. Possible reasons for the different behaviour are the details of the actuator, which is sinusoidal in the streamwise and uniform in the spanwise directions in the current study, unlike the setup of the aforementioned work where the actuator is not strictly spanwise homogeneous.

The spatial evolution of the skin friction relative to the unactuated boundary layer for different actuation amplitudes is presented in figure 4b. If the actuation amplitude is reduced from the baseline case $A^+ = 2$ to $A^+ = 1$ with the same actuation frequency the drag reduction drops below 5% and the flow recovers to the unactuated state within 200 viscous units downstream of the actuator. In contrast, when the amplitude is increased the results show that a significantly higher drag reduction can be achieved. For the case of an amplitude of $A^+ = 4$ this reduction is approximately a factor of two compared to the base line case of $A^+ = 2$ for $x^+ < 200$. However, further downstream the difference between both cases is negligible. If the actuation amplitude is increased even further to $A^+ = 6$ the initial reduction of skin friction is 40% at 50 viscous units downstream of the actuator with even higher values closer to the

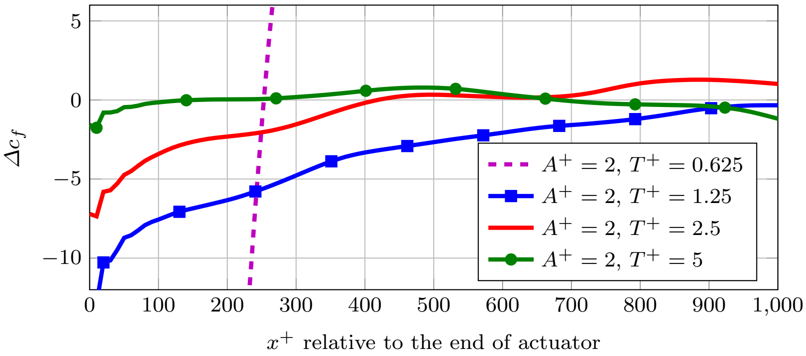

(a) Influence of different actuation frequencies on skin-friction with fixed actuation length of $L^+ = 375$ and actuation amplitude of $A^+ = 2$.

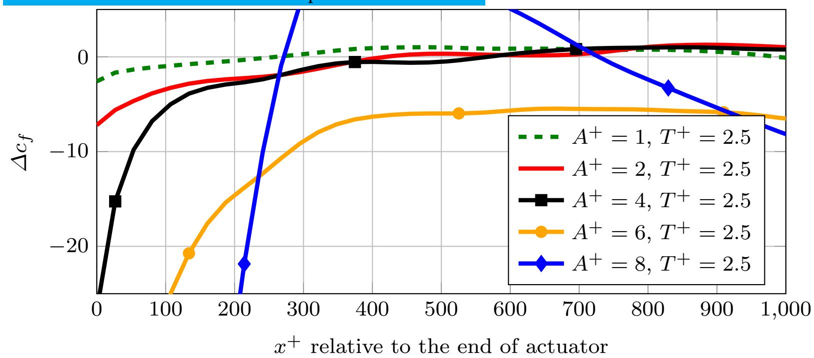

(b) Influence of different actuation amplitudes on skin-friction with fixed actuation length of $L^+ = 375$ and actuation period of $T^+ = 2.5$.

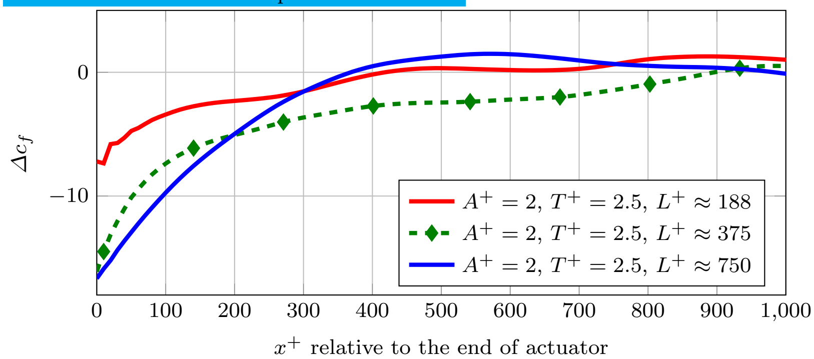

(c) Influence of actuator length on skin-friction with fixed actuation amplitude of $A^+ = 2$ and actuation frequency of $T^+ = 2.5$.

Fig. 4: Spatial evolution of skin friction downstream of the actuator for different actuation parameters. The viscous units used to scale the streamwise coordinate x were derived at the actuator end from the unactuated case.

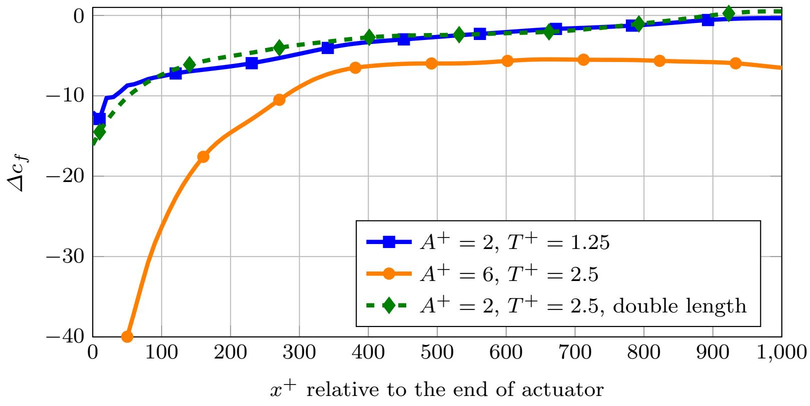

Fig. 5: Comparison of the difference in skin friction compared to the unactuated case for the most successful parameter sets.

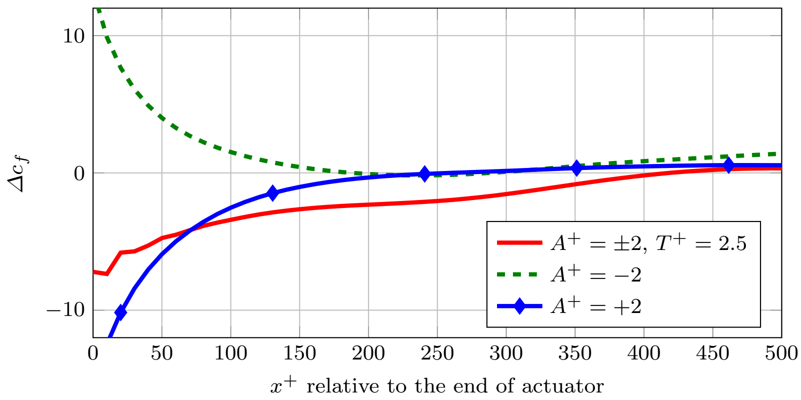

Fig. 6: Influence of stationary bump or dip compared to the baseline actuation of $A^+ = 2$, $T^+ = 2.5$.

actuator. In addition the behaviour changes qualitatively further downstream. Firstly the recovery towards the canoncial conditions is slower compared to the other cases. Furthermore the skin friction converges to a value that is more than 5% below the unactuated boundary layer. Indeed the value does not recover to the original level for the rest of the computational domain which ends 3530 viscous units downstream of the actuator. This is remarkable as it indicates that the boundary layer was not only locally disturbed but sustainably changed. For an actuation amplitude of $A^+ = 8$ the qualitative behaviour is comparable to the very fast actuation with $A^+ = 2$ and $T^+ = 0.625$. [1] found an optimum actuation amplitude of $A^+ = 2$ with less skin friction reduction for higher and lower amplitudes. This is in contrast to the results found in the current study where a higher amplitude leads to a higher skin friction reduction.

Finally the actuator length was varied for the baseline actuation parameters $A^+ = 2$, $T^+ = 2.5$. Figure 4c compares the Δc_f for three different actuator lengths. The data indicates that the actuator with a length of $L^+_{act} = 375$ seems to have the strongest influence on the skin friction of the boundary layer. Firstly, it leads to a high skin friction reduction in the direct vicinity downstream of the actuator. Secondly, and more importantly, the effect can be observed up to $x^+ = 900$ downstream of the actuator. If the actuator length is increased to $L^+_{act} = 750$ the initial Δc_f is slightly greater in magnitude up to $x^+ = 200$ downstream of the actuator but the recovery to the same values of the unactuated boundary layer is very similar to the baseline case.

The most successful control parameters are compared in figure 5. It is apparent that the fast actuation for an amplitude of $A^+ = 2$ has a similar effect to a case with twice the actuator length at a factor of two slower actuation. Overall the case with a high actuation amplitude of $A^+ = 6$ outperforms both of the other cases significantly with a higher peak skin friction reduction and showing a recovery converging to a lower value than the undisturbed boundary layer.

The investigation of different parameters is concluded with a stationary deflection of the actuator of $A^+ = 2$ in the form of either a bump or a dip. Both of these static deformations can be regarded as a singular roughness element. The change in skinfrction relative to the unactuated case is shown in figure 6. The negative amplitude, i.e. the dip, leads to an increase in skin friction until approximately $x^+ \approx 200$ downstream of the actuator. In contrast the positive deflection $A^+ = +2$ results in a reduction of skin friction almost symmetric to the increase observed in case of the dip. The comparison to the actuated case reveals that the skin friction reduction downstream of the actuator is greater for the stationary positive deflection for $x^+ < 80$. Downstream of this the flow recovers within approximately half the streamwise distance to the undisturbed state when no actuation is employed. The effect of a stationary bump or dip seems to be more significant in the direct vicinity of the actuator. However, in case of the actuation the flow is influenced significantly further downstream. This indicates that the effect of the unsteady wall-actuation is not due to stationary effects but a dynamic interaction of the actuation with the fluid flow. In this study, only the skin friction has been considered. In order to investigate the overall drag reduction potential of the wall-normal wall oscillation, the contribution from the pressure drag would need to be considered in addition.

4 Statistical examination of the most efficient cases

After the initial evaluation of the influence of the actuation on the skin friction of the turbulent boundary layer, this section compares other flow field statistics of the most efficient parameter sets with the non-actuated case.

Figure 7 compares the momentum thickness θ (7a) and the displacement thickness δ^* (7b) downstream of the actuator for the most efficient actuation parameters with the non-actuated boundary layer. It can be appreciated that for all actuated cases the momentum and displacement thickness just downstream of the actuator are lower than in the non-actuated case. This observation is crucial as it indicates that the change in skin friction observed for the actuated cases is due to a change in the turbulent flow and not due to a thickening of the boundary layer. The case with an actuation amplitude of $A^+ = 6$ and a period of $T^+ = 2.5$ showed a skin friction evolution that was not returning to the unactuated level. This case shows a thickening of the momentum thickness from 550 and a thickening of the displacement thickness from 370 viscous units downstream of the actuator, respectively. This indicates that the change in skin friction downstream of these locations can be predominantly attributed to a thicker boundary layer. However, for a zero pressure gradient boundary layer $\frac{\partial\theta}{\partial x} \approx c_f$ and therefore the higher gradient $\frac{\partial\theta}{\partial x}$ for the actuated case is unexpected. For the two other cases with the very fast actuation ($A^+ = 2$, $T^+ = 1.25$) and the actuator with the doubled length ($A^+ = 2$, $T^+ = 2.5$) the boundary layer only shows a minor thickening from approximately 700 viscous units downstream of the actuator. This location is in the region where the skin friction returns to the level of the unactuated case. In general, the case with the doubled actuator length shows the highest reduction in boundary layer thickness, indicating that the change in skin friction in that case is mainly related to changes in the turbulent flow.

Figure 7c shows the pressure at the wall for the most efficient actuation parameters in comparison with the unactuated case. The unactuated boundary layer features a pressure value that is approximately constant as it is expected for a zero pressure gradient boundary layer. For all actuated cases a lower pressure value can be observed downstream of the actuator. This reduced pressure slowly increases with the streamwise evolution of the boundary layer. As a result the pressure gradient is positive. The reduced pressure and adverse pressure gradient is particularly pronounced for the case with an actuation amplitude of $A^+ = 6$ and a period of $T^+ = 2.5$. This is consistent with the unexpected observation of the skin friction reduction despite an increased momentum thickness θ from $x^+ \approx 550$ downstream of the actuator and the higher $\frac{\partial\theta}{\partial x}$ in comparison with the unactuated boundary layer. As the flow downstream of the actuator is not a zero pressure gradient boundary layer, $\frac{\partial\theta}{\partial x} \approx c_f$ is no longer valid.

Figure 8a compares the streamwise velocity profiles in viscous units at $x^+ = 150$ downstream of the actuator. As a reference the $\widetilde{u_1}^+ = y^+$ and the

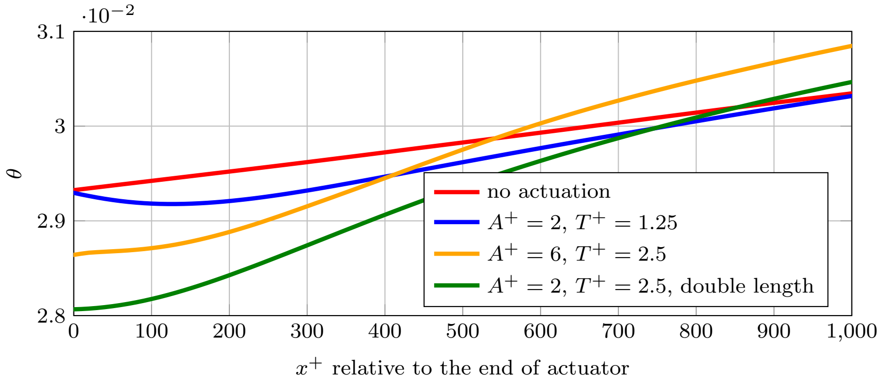

(a) Comparison of the momentum thickness θ for the most successful actuation parameters as a function of the streamwise location

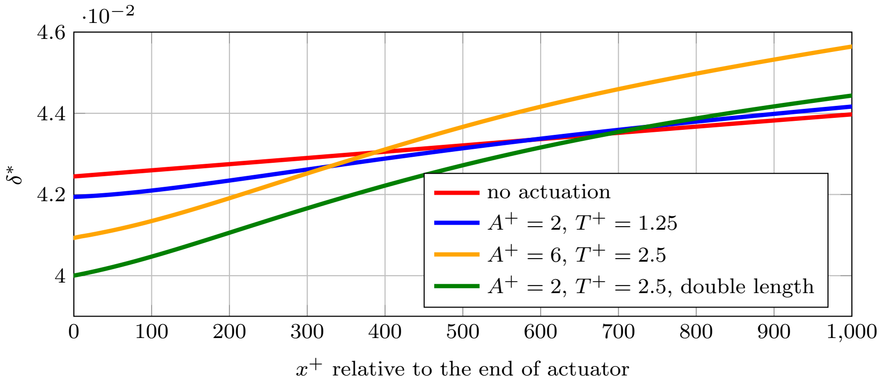

(b) Comparison of the displacement thickness δ^* for the most successful actuation parameters as a function of the streamwise location.

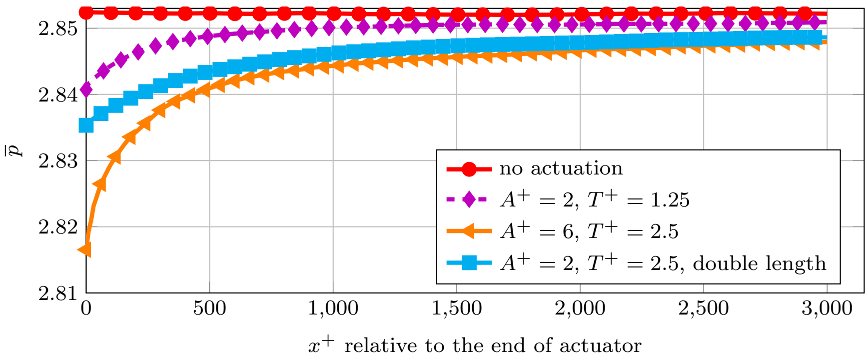

(c) Comparison of the pressure at the wall for the most efficient actuation parameters and the unactuated case downstream of the actuator.

Fig. 7: Boundary layer thickness and pressure at the wall downstream of the actuator for the most efficient actuation parameters.

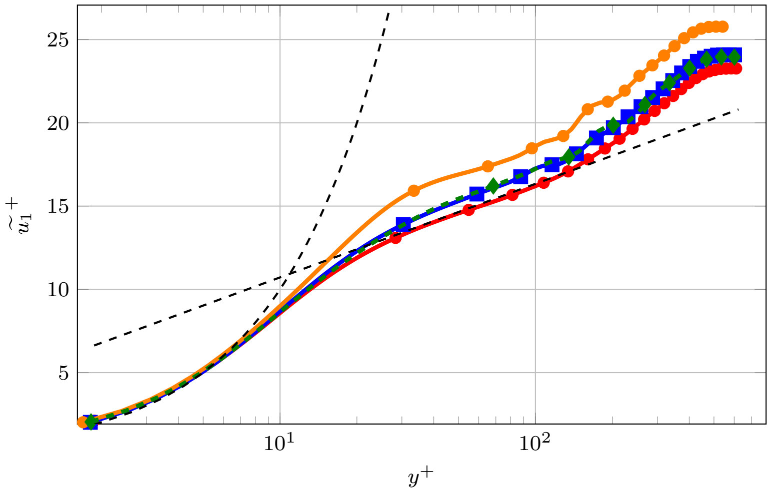

(a) Velocity profile in viscous scales.

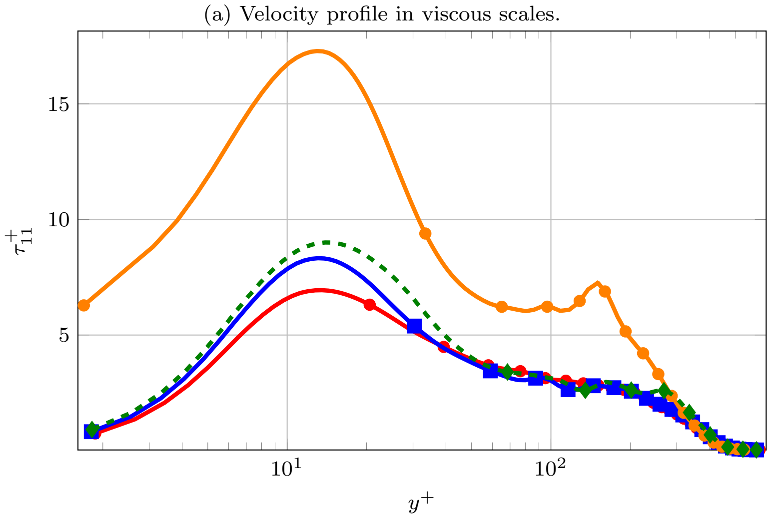

(b) Streamwise component of the Reynolds stress tensor.

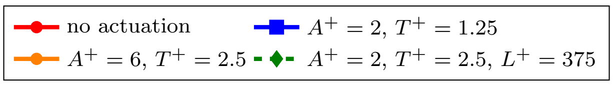

Fig. 8: Streamwise velocity mean and fluctuations at a streamwise position of 150 viscous units downstream of the actuator.

log-law are plotted in addition. All cases with actuation feature higher values from the logarithmic region to the freestream, which is consistent with the observed drag reduction. A shorter buffer layer as observed by Bai et al. [1] and other researchers can not be found in the current case, though.

The streamwise Reynolds stress component τ_{11} presented in figure 8b shows a significantly higher level when the actuation is employed. This is in particular true for the peak near the wall. For the two cases $A^+ = 2, T^+ = 1.25$ and $A^+ = 2, T^+ = 2.5, L^+ = 375$ the fluctuation levels are comparable to the unactuated case for wall distances $y^+ > 50$. For the most successful combination of actuation parameters $A^+ = 6, T^+ = 2.5$ this is not the case and the amplitudes are significantly higher at all wall distances with a second peak at $y^+ \approx 150$. This second peak was also observed in previous studies by Park & Choi [10] and Guo et al. [3] who used steady suction as well as blowing and a synthetic jet actuator, respectively. It should be mentioned that the relative difference between the cases can also be found without the inner scaling of the visous units.

For the highest actuation frequencies with an amplitude of $A^+ = 2$ and the highest actuation amplitude of $A^+ = 8$ at $T^+ = 2.5$ the maximum actuators' velocities were $u^+ = 20.1$, corresponding to $u_{act}/U_\infty = 1.1$ in outer scaling. In both cases high skin friction reductions were observed up to $x^+ = 220$ downstream of the actuator and, followed by a sharp increase to a higher value than without actuation. The spatial evolution of the skin friction for both parameter sets is compared to the case without actuation in figure 9a. In addition a simulation with the same maximum actuator velocity was carried out for an amplitude of $A^+ = 4$ and a period of $T^+ = 1.25$ which is also shown in the figure. From the evolution of the skin friction it can be concluded that the actuation leads to separated flow downstream of the actuator. Downstream of the reattachment point an increase in skin friction can be observed and it can be speculated that it is caused by the transport of high momentum from the freestream to the proximity of the wall by the separated flow. The topology of the separation bubble is visualized with the contours of the streamwise velocity component in figure 9c for the case with an actuation amplitude of $A^+ = 4$ and an actuation period of $T^+ = 1.25$. The streamlines and contours reveal that the separation bubble influences the flow up to a wall distance of approximately $y^+ = 20$. The streamwise velocity profiles at the end of the actuator and 60^+ units downstream of the actuator are compared in figures 9 for the three cases that exhibit a recirculation area. As above the streamwise coordinate x^+ refers to the same physical location in all cases as x is scaled with the viscous units from the unactuated case. It is found that the maximum recirculation bubble height is approximately 13 viscous units for the $A^+ = 2$ and $A^+ = 4$ cases. This maximum recirculation bubble height is reached downstream of the actuator end. The growth from the end of the actuator to the downstream location is small, though. For these two cases the separation bubble height is a factor of three to six above the actual actuation amplitude. The behaviour of the $A^+ = 8$ case is different in two regards: The recirculation bubble height only reaches the actuation amplitude at the end of the actuator and downstream of the actuator the recirculation bubble is reducing in height. Figure 10a shows the contours of the wall normal velocity component in the vicinity of the actuator for the baseline case. The contours show an area with relatively

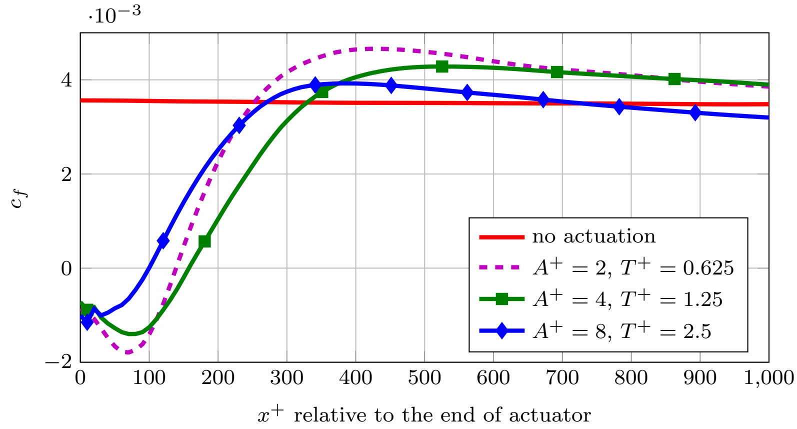

(a) Spatial evolution of skin friction for very fast actuation with a period close to the viscous time scale and a maximum actuation velocity of $u^+_{act} = 20.1$ which is equivalent to $u_{act}/U_\infty = 1.1$.

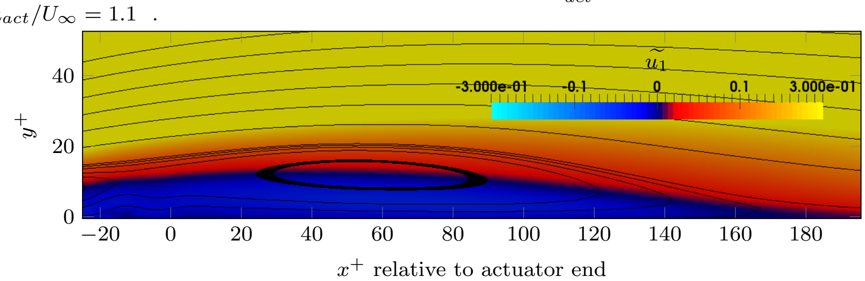

(b) Contours of the Favre-averaged streamwise velocity component in the vicinity of the actuator for the $A^+ = 4$ and $T^+ = 1.25$ case.

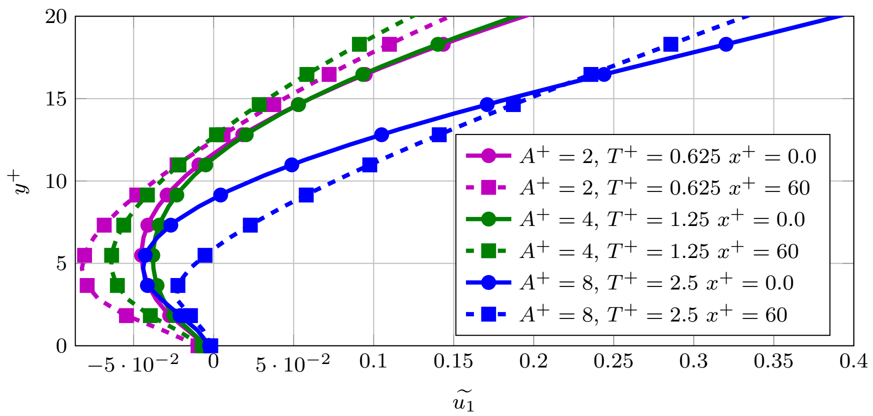

(c) Profiles of the streamwise velocity component at the actuator end and 60^+ units downstream of the actuator for three cases with recirculation.

Fig. 9: Examination of the two cases with the highest actuation velocities with the baseline actuator length.

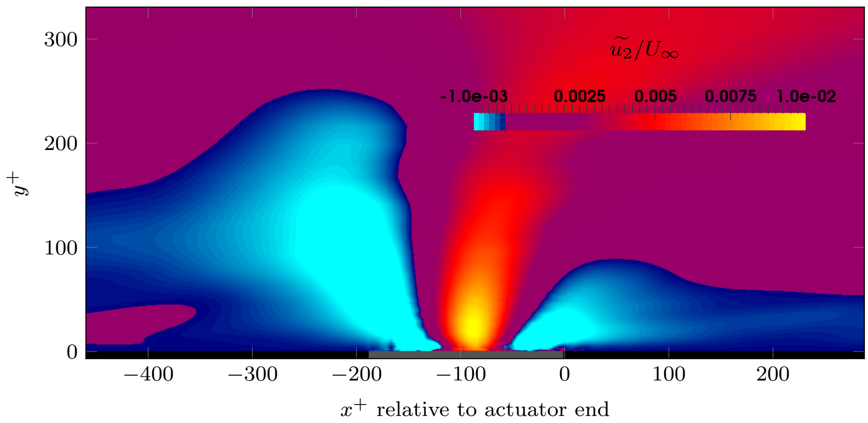

(a) Contours of wall normal velocity component for the case with $A^+ = 2$, $T^+ = 2.5$ and an actuator length of $L^+ = 188$. The location of the actuator is indicated in dark grey.

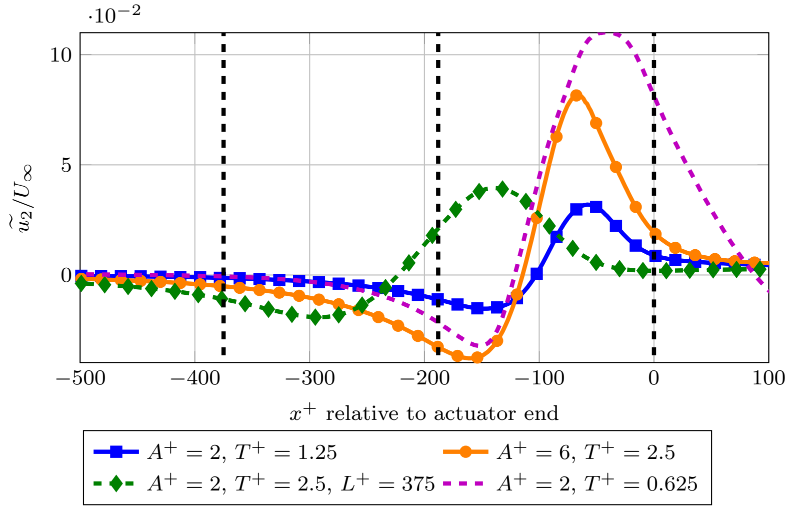

(b) Comparison of the wall normal velocity profile $\widetilde{u_2}$ at a wall distance of $y^+ = 75$ for the most successful actuation parameters. The vertical dashed lines indicate the actuator location for both actuator lengths with a common end point.

Fig. 10: Examination of the wall normal velocity in the vicinity of the actuator.

high velocity values that reaches from the wall at the center of the actuator to the freestream. This area is enclosed by areas with reversed flow towards the wall. The overall topology can be interpreted as a jet that originates from the center of the actuator and is non-symmetric and slightly inclined due to the cross flow of the freestream. The data shows that the periodic actuation on average is converted into a jet with a net momentum flux. This is similar to synthetic jet actuators (SJA) that in contrast to the current setup feature a cavity below the wall where the actual actuation occurs. Such devices were also used by [3] within a spanwise slot for flow control of a turbulent boundary layer.

Figure 10b compares the crosssection velocity profiles of the jets at a wall distance of $y^+ = 75$ for the most successful actuation parameters and one parameter set where separation downstream of the actuator was observed. The peak velocity value is not symmetric with respect to the center of the actuator and is shifted towards the downstream direction. Comparing the actuated cases the parameters that showed the greatest reduction in the skin friction coefficient c_f also produced the strongest jet. This indicates that the formation of the wall-normal jet is essential for a drag reduction, with greater reductions for stronger jets which also results in an adverse pressure gradient downstream of the actuator, as presented in figure 7c. However, if the jet is too strong, as for the $A^+ = 2, T^+ = 0.625$ case, the flow separates downstream of the actuator. In fact all other cases that featured a separation bubble which are not shown here have peak values $\widetilde{u_2} > 0.1 u_\infty$.

5 Conclusions

The effect of spanwise homogeneous wall normal periodic actuation on a turbulent boundary layer was investigated numerically, using direct numerical simulations combined with a boundary data immersion method. The results indicate that the effect of the actuation increases with increasing frequency and amplitude up to a certain point. It could be shown that the skin friction reduction that was observed is not only related to a thickening of the boundary layer, but is a consequence of an interaction between the actuator and the turbulent boundary layer. The examination of the averaged velocity fields revealed that the actuation results in a non-zero momentum-flux wall-normal jet, despite there being no plenum or cavity as in commonly studied synthetic jet actuators. However, for all actuated cases where the maximum velocity of the actuation exceeded $u^+_{act} = 20.1$ or $u_{act}/U_\infty = 1.1$ the flow separated downstream of the actuator. The stronger this jet is the greater its effect on the skin friction downstream of the actuator.

Acknowledgements This research was undertaken with the assistance of resources provided at the NCI National Facility systems at the Australian National University through the National Computational Merit Allocation Scheme supported by the Australian Government. Furthermore this work was supported by resources provided by The Pawsey Supercomputing Centre with funding from the Australian Government and the Government of Western Australia.

Compliance with Ethical Standards: The authors declare that they have no conflict of interest.

References

1. Bai, H., Zhou, Y., Zhang, W., Xu, S., Wang, Y., Antonia, R.A.: Active control of a turbulent boundary layer based on local surface perturbation. Journal of Fluid Mechanics **750**, 316–354 (2014)
2. Endo, T., Kasagi, N., Suzuki, Y.: Feedback control of wall turbulence with wall deformation. International Journal of Heat and Fluid Flow **21**(5), 568–575 (2000)
3. Guo, H., Huang, Q.M., Liu, P.Q., Qu, Q.L.: Effects of local high-frequency perturbation on a turbulent boundary layer by synthetic jet injection. Fluid Dynamics Research **47**(4), 45,501 (2015)
4. Hurst, E., Yang, Q., Chung, Y.: The effect of Reynolds number on turbulent drag reduction by streamwise travelling waves. Journal of Fluid Mechanics **759**, 28–55 (2014)
5. Itoh, M., Tamano, S., Yokota, K., Taniguchi, S.: Drag reduction in a turbulent boundary layer on a flexible sheet undergoing a spanwise traveling wave motion. Journal of Turbulence **7**(27), 1–17 (2006)
6. Jacobson, S., Reynolds, W.: Active control of streamwise vortices and streaks in boundary layers. Journal of Fluid Mechanics **360**, 179–211 (1998)
7. Kang, S., Choi, H.: Active wall motions for skin-friction drag reduction. Physics of Fluids **12**(12), 3301 (2000)
8. Lardeau, S., Leschziner, M.: The streamwise drag-reduction response of a boundary layer subjected to a sudden imposition of transverse oscillatory wall motion. Physics of Fluids **25**(7), 075,109 (2013)
9. Nagamine, H., Yamahata, K., Hagiwara, Y., Matsubara, R.: Turbulence modification by compliant skin and strata-corneas desquamation of a swimming dolphin. Journal of Turbulence **5**(18) (2004)
10. Park, J., Choi, H.: Effects of uniform blowing or suction from a spanwise slot on a turbulent boundary layer flow. Physics of Fluids **11**(10), 3095–3105 (1999). DOI 10.1063/1.870167. URL http://link.aip.org/link/PHFLE6/v11/i10/p3095/s1
11. Sandberg, R.: Compressible-Flow DNS with Application to Airfoil Noise. Flow, Turbulence and Combustion **95**(2), 211–229 (2015)
12. Sandberg, R., Sandham, N.: Nonreflecting zonal characteristic boundary condition for direct numerical simulation of aerodynamic sound. AIAA Journal **44**(2), 402–405 (2006)
13. Schlanderer, S., Weymouth, G., Sandberg, R.: The boundary data immersion method for compressible flows with application to aeroacoustics. Journal of Computational Physics **333**(15), 440–461 (2017)
14. Schlatter, P., Örlü, R.: Assessment of direct numerical simulation data of turbulent boundary layers. Journal of Fluid Mechanics **659**, 116–126 (2010)
15. Schlatter, P., Örlü, R.: Turbulent boundary layers at moderate Reynolds numbers: inflow length and tripping effects. Journal of Fluid Mechanics **710**, 5–34 (2012)
16. Serrano Galliano, S., Sandberg, R.: Effect of the leading and trailing edge geometry on the fluid-structural coupling of membrane aerofoils. In: 2016 AIAA SciTech. AIAA Paper 2016-0853 (2016)
17. Tamano, S., Itoh, M.: Drag reduction in turbulent boundary layers by spanwise traveling waves with wall deformation. Journal of Turbulence **13**(9) (2012)
18. Touber, E., Sandham, N.: Large-eddy simulation of low-frequency unsteadiness in a turbulent shock-induced separation bubble. Theoretical and Computational Fluid Dynamics **23**, 79–107 (2009). DOI 10.1007/s00162-009-0103-z
19. Yanagimoto, K., Yamamoto, S., Kawazoe, H., Hamamoto, N.: Research on Skin Friction Drag Reduction by Vibrant Wall. Journal of Fluid Science and Technology **6**(4), 625–636 (2011)